INTERNATIONAL JOURNAL OF HYDROGEN ENERGY 42 (2017) 24785–24796

Available online at www.sciencedirect.com

ScienceDirect

journal homepage: www.elsevier.com/locate/he

Influence of carbon support properties on the electrocatalytic activity of PtRuCu nanoparticles for methanol and ethanol oxidation

Vanina Comignani [a], *Juan Manuel Sieben* [a,*], *Miguel D. Sanchez* [b], *Marta M.E. Duarte* [c]

[a] *Instituto de Ingeniería Electroquímica y Corrosion and CONICET, Universidad Nacional del Sur (UNS), Av. Alem 1253 Bahía Blanca B8000CPB, Argentina*

[b] *Instituto de Física del Sur (IFISUR), Departamento de Física, Universidad Nacional del Sur (UNS), CONICET, Av. Alem 1253 Bahía Blanca B8000CPB, Argentina*

[c] *Instituto de Ingeniería Electroquímica y Corrosion and CIC, Universidad Nacional del Sur (UNS), Av. Alem 1253 Bahía Blanca B8000CPB, Argentina*

ARTICLE INFO

Article history:
Received 21 June 2017
Received in revised form
11 August 2017
Accepted 12 August 2017
Available online 4 September 2017

Keywords:
PtRuCu nanoparticles
Carbon materials
Surface oxidized supports
Methanol and ethanol oxidation

ABSTRACT

This work set out to explore the influence of kind and surface condition of carbon supports on the electrocatalytic activity of trimetallic PtRuCu alloy nanoparticles. The structure, composition, particle size and catalyst loading were determined by XRD, EDX, XPS, TEM and ICP-AES analysis. XRD studies revealed that support physical characteristics and surface conditions have an important influence in lattice strain, while XPS pointed out that a strong electronic interaction exists between the particles and the carbon support. Electrochemical experiments showed that the activated carbon black supported PtRuCu catalyst exhibits the best performance for methanol and ethanol oxidation and the lowest poisoning rate. The superior catalytic activity of this electrode can be rationalized in terms of metal-support interaction, Pt utilization efficiency and electrical conductivity of the carbon support. Furthermore, the as-prepared electrode exhibits 13 and 7 times higher activity towards methanol and ethanol oxidation when compared with a PtRu/C commercial catalyst.

Introduction

Methanol and ethanol are proposed as alternative fuels for low-temperature polymer electrolyte membrane fuel cells because they have high energy density (ca. 6–9 kW h kg^{-1}) and are easier to transport and distribute to the public using the current infrastructure [1]. Besides, these alcohols can be produced directly or indirectly from agricultural and forestry wastes, industrial residues, municipal solid waste and animal residues, which in turn may help to reduce the carbon dioxide emissions to the atmosphere [2–4].

The direct alcohols fuel cells are considered the most appropriate substitutes for rechargeable batteries in low power mobile and portable devices such as handheld

* *Corresponding author.*
E-mail address: jmsieben@uns.edu.ar (J.M. Sieben).
http://dx.doi.org/10.1016/j.ijhydene.2017.08.079

cameras, mobile phones, portable computers, portable radios, medical equipment, etc., which are sold in millions allover the world [5,6]. Today, however, the widespread production and global commercialization of liquid-feed direct alcohol fuel cell stacks is limited by the high cost of Pt, high fuel permeability through the ionomer membrane (i.e., crossover phenomenon) and deficient activity, selectivity and low stability of anode electrocatalysts at low operating temperatures.

A new approach to obtain highly selective and active electrocatalysts with low noble metals loading for methanol oxidation reaction (MOR) and ethanol oxidation reaction (EOR) involves the preparation of multifunctional nanostructured particles [7–12]. For instance, recent investigations on atomically ordered Ru@Pt [9] and Ni@Pt-Ru [12] core–shell nanoparticles have suggested enhanced activity, selectivity and durability with respect to PtRu/C and Pt/C catalysts in the operating conditions of direct methanol fuel cells (DMFC). Other work has shown that trimetallic PtRuCu alloy nanoparticles with surface defects present improved activity towards methanol oxidation compared to similar sized PtRu particles [10]. Most recently, Cao and co-workers have successfully synthesized PtCu hierarchical branched nanoparticles with greatly enhanced electrocatalytic performance for methanol oxidation in comparison to a commercial PtRu/C material [11]. The superior electrocatalytic performance of these nanoparticles can be rationalized on the basis of lattice strain effects, modification of the electronic surface structure and high efficiency of Pt utilization. On the other hand, carbon support nature and state are known to play a crucial role on the activity of supported catalysts influencing not only particle morphology, size and distribution but also modifying the electronic structure of the catalyst. For instance, the graphitization degree (i.e., extension of the sp^2 network) [13], presence of surface functionalities [14,15] and doping with heteroatoms (N, S, P, B) [16,17] affect effectiveness and extent of electron transfer from particles to support. On the other hand, textural and morphological characteristics (i.e. specific surface area, porosity, etc.) of support materials also affect catalyst activity and selectivity towards methanol and ethanol oxidation [18].

Therefore, the main objective of this work is to study the influence of structural characteristics and surface composition of two widely different carbon supports on the electrocatalytic activity of trimetallic PtRuCu alloy nanoparticles towards methanol and ethanol electro-oxidation in acid medium. The supported trimetallic alloy nanoparticles have been synthesized by a two-step preparation method and characterized by different physicochemical techniques. Previous studies have determined that this trimetallic systems have high catalytic activity for the oxidation of methanol and ethanol in acid medium [19,20].

Experimental

Reagents and carbon supports

Carbon black from Cabot (Vulcan XC-72R, particle diameter about 40 nm, labeled as CG) and multi-walled carbon nanotubes from Aldrich (MWCNTs, ≥98%, carbon, outer diameter ca. 10 nm and length between 3 and 6 μm, labeled NT) were used as supports. These carbonaceous materials were treated with 3.0 M HNO_3 solution at 60 °C for 3 h. The slurry was then cooled and its pH value was adjusted to 7.0 with 1.0 M NaOH solution. The pretreated carbon materials (labeled as CGA and NTA) were then filtered, rinsed thoroughly with bidistilled water and ethanol, and dried in an oven at 80 °C overnight.

Hexachloroplatinic (IV) acid hexahydrate ($H_2PtCl_6 \cdot 6H_2O$, 40 wt % Pt) was purchased from Sigma-Aldrich, while anhydrous copper (II) sulfate ($CuSO_4$, p.a.) and ruthenium (III) chloride hydrate ($RuCl_3 \cdot xH_2O$, 41 wt % Ru) were obtained from Merck. Sodium hydroxide (NaOH, ≥ 97.0%) and sodium borohydride ($NaBH_4$, >94%) were also supplied by Sigma-Aldrich. Sulfuric acid (96 wt %) and hydrochloric acid (37 wt %) were obtained from Carlo Erba, while CH_3OH (99.9%), CH_3CH_2OH (99.9%) and isopropyl alcohol (>99.5%) were provided by J.T. Baker®. In addition, Nafion® 117 solution (5 wt % in a mixture of lower aliphatic alcohols and water) was supplied by Sigma-Aldrich. All solutions were prepared with tridistilled water.

Catalysts preparation

The trimetallic nanoparticles supported on the different carbon materials were synthesized via a two-step reduction process. Ru-Cu particles were prepared by dissolving $RuCl_3$ and $CuSO_4$ salts in 50 mL of 0.25 M HCl and then adding to an aqueous carbon support suspension (2 mg mL^{-1}). After 45 min constant stirring solid $NaBH_4$ was slowly added to the mixture in a weight ratio of 5:1, and left to react for 2 h under moderate stirring. The resulting metal-carbon material was collected via suction filtration, washed thoroughly with bidistilled water and ethanol and then redispersed in 50 mL of bidistilled water by sonication for 30 min. The nominal Cu and Ru metal loading on carbon was 22.2 and 11.1 wt %, respectively. Then, 2.65 mL of 0.0386 M $H_2PtCl_6 \cdot 6H_2O$ aqueous solution (11.1 wt % of Pt on carbon) was added to the suspension and left to react for 2 h under moderate stirring. The solid product that remained at the end of the reaction was recovered via suction filtration, washed with water and ethanol and dried in an oven overnight.

Physicochemical characterization

Nitrogen isotherms were determined at −196 °C using a Nova 1200e Quantachrome instrument after degassing the produced chars at 150 °C until outgassing was completed. The specific surface area of the carbonaceous materials was calculated by the BET equation. The total micropore volume (V_{DR}-N_2) was calculated from the application of the Dubinin–Radushkevich equation to the N_2 adsorption at −196 °C.

Carbonaceous materials conductivity was measured on pellets by using PVDF as binder (5 wt % of the pellet weight). The pellets of about 0.5 cm in diameter and ca. 1.5 mm in thickness were obtained after pressing at 0.1 Ton cm^{-2} at room temperature for 5 min. Electrical conductivity was calculated according to $\sigma = h/(R \times A)$; where R is the resistance measured, h is the pellet thickness and A is the circular surface area. The procedure used to measure the ohmic resistance of the samples was similar to that reported elsewhere [21,22]. To ensure reproducibility, ohmic resistance was

measured for three different samples of each carbon material at a pressure of 150 kPa.

X-ray diffraction (XRD) patterns of the catalysts were collected on a Rigaku Dmax III C diffractometer with monochromated CuKα radiation source operated at 40 keV at a scan rate of 0.05° s^{-1}. The bulk composition of the samples was determined on a scanning electronic microscope (SEM) LEO 1450 VP equipped with an energy dispersive X-ray probe (EDX), EDAXGenesis 2000. The microstructure of the as-synthesized materials was analyzed on a transmission electronic microscope (TEM) JEOL 100CX II.

X-ray photoelectron spectroscopy (XPS) measurements and analyses were performed in a PHI 548 spectrometer whit a Double Pass Cylindrical Mirror Analyser, using the Al Kα non-monochromatic radiation at 300 W and 20 mA. The resolution spectra were taken at 50 eV of pass energy, giving an absolute resolution of about ±0.5 eV. The operation base pressure were better than 5×10^{-9} Torr. The C 1s binding energy was taken as a charge reference and fixed at 285.0 eV. The signal deconvolution was made using Shirley type background subtraction and sum of Gaussian–Lorentzian functions. The atomic ratio estimations were done relating the peak areas after the background subtraction and corrected relative to the corresponding atomic sensitivity factors to an approximated absolute error of 20%.

The amount of the metals deposited on the carbon supports was determined by inductively coupled plasma atomic emission spectrometry (ICP-AES, Shimadzu 1000 model III).

Electrochemical characterization

The electrochemical measurements were performed at room temperature with a PAR 273 potentiostat/galvanostat using a Pt wire as counter electrode and a saturated calomel electrode (SCE, +0.241 V vs. NHE) as the reference electrode. All potentials mentioned in this work are referred to this electrode. The working electrodes were prepared by dispersing 20 μL of a catalyst ink over the surface of a polished glassy carbon rod (0.07 cm^2). Then, the electrodes were dried at 60 °C for 30 min with an IR-lamp to ensure the catalyst binding to the glassy carbon support. The catalyst ink was prepared by following the procedure described elsewhere [23]. Briefly, the inks of the as-prepared catalysts were made by ultrasonically blending 20 mg of powder samples, 7.96 mL of tridistilled water, 2 mL isopropyl alcohol and 40 μL Nafion ionomer solution for 30 min.

The catalytic performance of the as-prepared electrodes for the electro-oxidation of 1 M methanol (MeOH) and 1 M ethanol (EtOH) was determined in 0.5 M H_2SO_4 solution by electrochemical techniques such as cyclic voltammetry (CV) and chronoamperometry (CA). Before starting the experiments, all solutions were deaerated by bubbling N_2 for 30 min and then the inert atmosphere was maintained over the solution during the tests. The CV experiments were conducted applying a potential sweep of 50 mV s^{-1} in a potential window of −0.2–0.9 V (vs. SCE). The steady state voltammograms were obtained after 30 cycles, whereas the stationary measurements were performed applying pulses of 0.4 and 0.5 V for 900 s. Current densities for alcohols electro-oxidation were normalized per milligram of Pt. The active surface area of the electrocatalysts (ECSA) was estimated by CO stripping experiments by following the procedure described in a previous paper [24]. A commercial Pt-Ru/C electrocatalyst from Sigma Aldrich (20 wt % Pt and 10 wt % Ru loading, ECSA = 60.3 m^2 g^{-1} and d_p = 2.9 nm) was used for comparison [23].

Results and discussion

Carbon supports characterization

Table 1 shows the BET surface areas calculated from N_2 adsorption data at −196 °C [VDR (N_2)] and the electrical conductivity of all carbon supports. The carbon materials exhibit Type II isotherms, which are characteristic of systems containing micropores and also macropores attributed to particle agglomeration [25,26]. The BET surface area of CG was measured as 228 m^2 g^{-1} while the multiwalled carbon nanotubes presented a BET surface area up to 2.6 times higher than the other supports (335 m^2 g^{-1}). These values are comparable to results published in the literature [27,28]. Contrary to expectations, the highly conductive multiwalled carbon nanotubes presented lower conductivity values than carbon black. This result is likely related to differences in the contact area and packing density of the particles under compression, which in turns influences contact resistance [21]. Therefore, we presume that the contact resistance of the carbon black powder is smaller than that of the nanotubes in the experimental setup used for the measurements. Marinho et al. indicated that the contact resistance influence is far more pronounced in nanotubes than in carbon black, especially at low applied pressures [21].

In addition, it can be noted that the BET surface area and the porosity decreased about 50% after the chemical oxidation pretreatment of the pristine carbon materials due to the corrosion of the pore walls that causes a damage in the porous structure. This behavior is in line with the results reported in the bibliography [29–31]. On the other hand, the electrical conductivity was found also to decrease after the pretreatment. Specifically, CG and NT conductivity was reduced by a factor of three after the pretreatment due to the reduction of the graphitic domains. A possible explanation is that the oxidative treatment partially destroys the conjugated sp^2 network and the carbon atoms decorated with oxygen functionalities adopt sp^3 hybridization. Therefore, the electron transference at the surface of the particles becomes much more difficult and the interfacial resistance between the particles augments.

Furthermore, oxygen atomic content at the near surface of the different carbonaceous materials was determined by XPS

Table 1 – Porous texture, electrical conductivity and surface elemental composition of carbon supports.

Material	A_{BET} (m^2 g^{-1})	V_{DR}-N_2 (cm^3 g^{-1})	σ (S cm^{-1})	C (at. %)	O (at. %)
CG	228	0.36	1.395	92.9	1.4
CGA	92	0.34	0.383	90.5	4.2
NT	335	0.60	0.033	90.0	2.3
NTA	177	0.20	0.011	88.7	9.0

analysis. As can be seen from Table 1, the relative percentage of oxygen raised appreciably for both CG and NT after the mild oxidation treatment with HNO_3. The oxidation procedure increased the atomic oxygen concentration by about 200 and 290% on the surface of CG and NT, respectively, i.e., the surface oxidation degree of NT was higher than that of CG. Fig. 1 shows the O 1s core level spectra for the raw carbon materials and the acid-treated samples. The XPS signal can be deconvoluted into three peaks at BEs of 535.4 eV, 533.6 eV and 532.1 eV. The peak centered at 532.1 eV is assigned to the presence of carbonyl or quinone type groups, the peak located at 533.6 eV is attributed to oxygen single bonded to carbon (phenol, lactones or anhydrides) and the shoulder that appears at 535.4 eV is probably associated with the presence of chemisorbed water [32,33]. At first inspection we can note that on CG the intensity of the peak ascribed to carbon atoms bonded with hydroxyl and epoxy group is higher than that attributed to C=O species, which indicates that the C-OH species are the dominant functional groups. On the contrary, the O 1s spectrum of NT shows that the contribution of the double bonded species is found to be higher than that of the single bonded groups. Oxidation of CG results in increase of the relative amount of carbonyl and quinone groups, while oxidation of NT results in increase of the percentage of phenols and ethers functionalities. These results suggest that the surface oxidation of CG and NT samples proceed via different mechanisms and it is consistent with literature reports attributing this difference to the degree of interlayer interaction between graphene sheets [34].

Catalysts characterization

After the synthesis the supported catalysts were characterized by TEM. Fig. 2 shows the TEM images and corresponding particle size distribution histograms of the trimetallic PtRuCu nanoparticles supported over the different carbonaceous materials. The average particle size of the as-synthesized catalysts is included in Table 2. As shown in the micrographs, the different carbons appear to be covered with nanoparticles ranging between 2.9 and 4.8 nm in diameter,

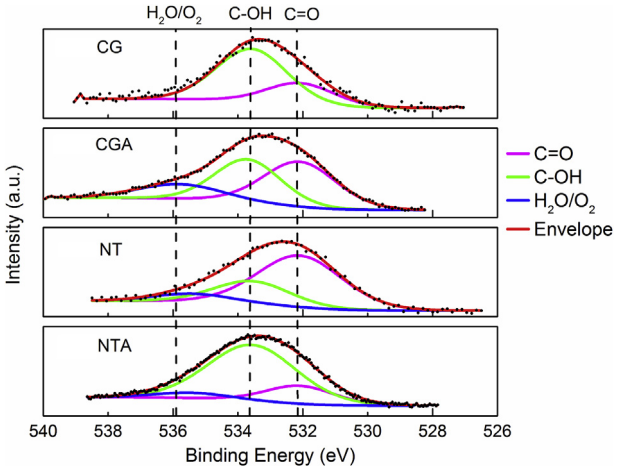

Fig. 1 – O 1s core level XPS spectra of the different carbon supports.

and small agglomerates (ca. 15 nm) comprised of smaller particles. The nanoparticles deposited on CG and NT supports have mean diameters of 2.9 nm and 4.5 nm with median values of 2.66 and 3.93 nm, respectively. As regard of CGA the mean diameter of the PtRuCu particles is 3.5 nm with a median of 3.1 nm, while the particles observed in the micrograph of PRC/NTA have a mean diameter of 4.3 nm with a median of 4.0 nm. It can be noted that the specific surface area and pore size distribution of the supports do not directly influence particle size and distribution and agglomeration degree of the trimetallic catalysts. The better particle distribution and lower particle size of PRC/CG with respect to PRC/NT catalyst may be probably attributed to the higher amount of hydroxyl and epoxy groups on the Vulcan XC-72R surface because these moieties can act as more effective anchoring sites for the growth of particles than carbonyl functionalities. On the other hand, TEM images reflect the effect of the oxidative pretreatment of the carbon support on the uniformity of the size distribution, dispersion and degree of agglomeration. Overall, the catalysts prepared with the pretreated carbon supports presented better particle dispersion and less agglomerates than those prepared with the pristine powdered carbon black and carbon nanotubes because the oxygen surface groups act as anchoring sites for immobilizing Cu and Ru precursors via electrostatic, coordinative and Van der Waals interactions. Fig. 2d also shows damage to nanotubes walls (i.e., broken walls and surface defects) caused by the oxidative pretreatment.

The XRD diffraction patterns of the different catalysts are illustrated in Fig. 3. All samples present three main Bragg peaks characteristic of the fcc structure of platinum located at angles of about 40°, 47° and 68°. This means that reduced copper and ruthenium atoms do not exist as individual particles on carbon substrates. The diffractograms show broader peaks and present a slight shift towards higher angles respect to corresponding peaks in pure Pt/C pattern (not shown). According to Table 2 and Fig. 3, a relationship between peak broadening and decreasing crystallite size can be observed. In addition, the slight shift towards higher angles of the diffraction peaks is probably caused by the formation of an alloy phase between Pt, Ru and Cu according to the Vegard's law, consequence of metals atoms interdiffusion across the interfacial vacancy defects created during the galvanic replacement reaction [19,35]. The lattice strain (ε) in the trimetallic PtRuCu particles relative to bulk Pt (lattice constant of 3.921 Å), is determined by the following expression [7,36]:

$$\varepsilon = \left(\frac{a_{CuRu@Pt} - a_{Pt}}{a_{Pt}} \right) \times 100 \quad (1)$$

The ε values are summarized in Table 2. The lattice strain of the nanoparticles deposited over NT is almost 20 times higher than on CG, effect that cannot be attributed to particle size effects because lattice strain decreases with increasing particle size [37]. Probably, the difference observed in ε values can be ascribed to morphological and textural properties of the supports. The oxidation of the carbon supports results in a higher extent of lattice strain, although the increase of ε in carbon black is much higher than in carbon nanotubes, Recently, Daio et al. [38] studied the influence of the support material on the evolution of lattice strain in Pt nanoparticles,

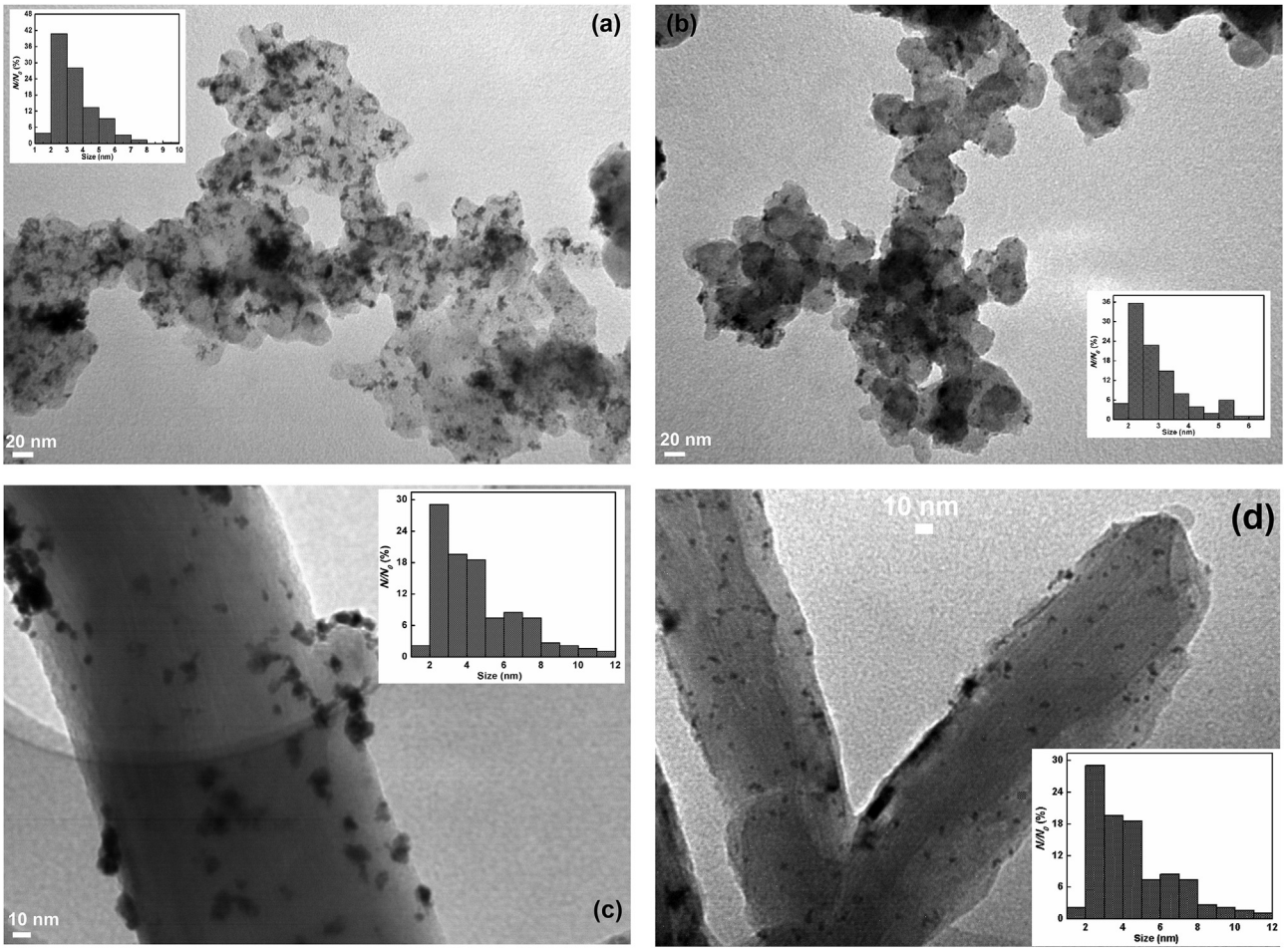

Fig. 2 – TEM Images and particle size histograms of trimetallic nanoparticles on different substrates. PRC/CG (a), PRC/CGA (b), PRC/NT (c) and PRC/NTA (d).

founding that the stronger the metal-support interaction, the higher the lattice strain. In this case, the metal atoms interact strongly with the oxygen moieties formed on the carbon surface after the oxidative pretreatment, which in turn induces a higher strain in the PtRuCu nanoparticles. In other words, the metal–oxygen moieties interaction does not only influence the size, dispersion, and chemical state of the catalyst particles, but also creates more strain in the supported nanoparticles.

EDX analysis confirmed that the as-synthesized nanoparticles supported over the different carbonaceous materials contain platinum, ruthenium and copper. The atomic composition of all samples is compiled in Table 3. With the exception of PRC/NT, the atomic ratio of Pt:Ru:Cu in the nanoparticles bulk was found to be about 1:1:1 which is different than the initial atomic ratio of salts precursors (1:2:6). The decreased amount of Cu is a consequence of the partial galvanic replacement reaction during the synthesis

Table 2 – Characteristic parameters of particles.

Catalyst	[a] d_p (nm)	[b] d_c (nm)	[c] a (Å)	ε (%)
PRC/CG	2.9 ± 0.3	2.6	3.917	−0.09
PRC/CGA	3.5 ± 0.7	3.4	3.853	−1.75
PRC/NT	4.5 ± 1.0	3.7	3.852	−1.77
PRC/NTA	4.1 ± 0.7	3.5	3.839	−2.09

[a] Average particle size (TEM).
[b] Crystallite diameter (XRD).
[c] Unit cell parameter.

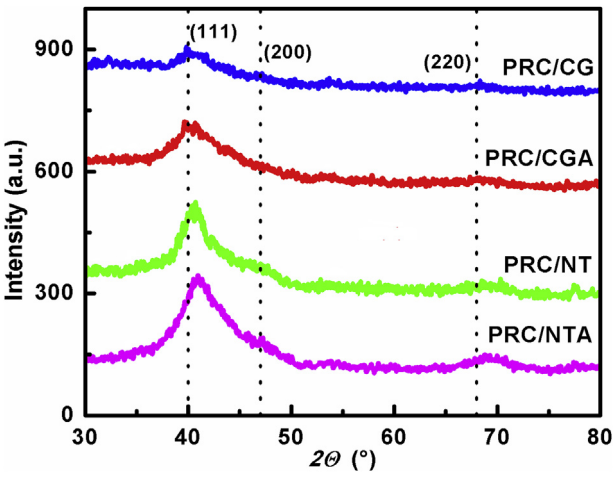

Fig. 3 – XRD patterns of the as-prepared PtRuCu catalysts.

Table 3 – Binding energies and relative contents of Pt, Ru and Cu in catalysts.

Sample	Binding energy (eV)				XPS (at. %)			EDX (at. %)		
	Pt $4f_{7/2}$	Ru $3d_{5/2}$	Ru $3p_{3/2}$	Cu $2p_{3/2}$	Pt	Ru	Cu	Pt	Ru	Cu
PRC/CG	71.3	281.5	462.3	932.0	34.2	44.6	21.2	29.8	32.4	37.8
PRC/CGA	71.3	281.2	461.9	931.9	37.5	39.3	23.2	25.5	26.3	48.3
PRC/NT	71.2	281.3	462.1	931.8	30.4	40.4	29.2	42.6	38.7	18.7
PRC/NTA	70.9	282.4	462.7	933.6	34.3	41.2	24.5	30.5	33.9	35.7

process. On the other hand, the amount of Ru was lower than expected from the initial precursor mass probably because a significant quantity of Ru atoms are detached from the surface of the Cu-Ru nanoparticles during the partial galvanic replacement reaction.

On the other hand, the composition and the chemical state of the surface atoms were evaluated by XPS. Fig. 4 displays the XPS high-resolution spectra corresponding to the regions of Pt, Cu, Ru and C different core levels and Table 3 shows the binding energies and the atomic surface composition obtained from deconvoluted spectra. Interestingly, it can be seen that the atomic composition on the surface and the near surface regions are slightly different to the bulk composition of the nanoparticles.

Fig. 4a shows the Pt 4f core level spectra of the as-prepared catalysts. Note the signals overlapped with Cu 3p and Ru 4s, whose signals were synthesized from those obtained for the regions of Cu $2p_{3/2}$ and Ru $3p_{3/2}$, Fig. 4c and d respectively. The peaks located around 71 and 74 eV are assigned to the Pt $4f_{7/2}$ and Pt $4f_{5/2}$ of metallic Pt, respectively. The Pt $4f_{7/2}$ peaks energy positions of the as-prepared samples are in good agreement with the expected for metallic Pt in bulk samples [39]. The position of the $4f_{7/2}$ peak in Pt/C and PtRu/C is marked with a dashed line located at 71.1 eV [40–42]. As noted, the Pt $4f_{7/2}$ peak of the as-prepared samples is shifted to the right compared to Pt/C and PtRu/C [40–42], suggesting electronic interaction between the surface and near surface Pt atoms and the other metals in the surface alloy, and/or the interaction between Pt and the carbon support [9,43,44]. Furthermore, the Cu $2p_{3/2}$ signal (Fig. 4b) can be deconvoluted into two peaks located at binding energies of about 932.0 and 933.7 eV. The main peak at 932.0 eV is ascribed to the presence of metallic Cu expected at 932.7 eV for bulk samples while the peak at 933.6 eV is associated with the presence of CuO in agreement with the expected value for bulk material [45]. It is interesting to note the shift between 0.7 and 1.1 eV to the lower binding

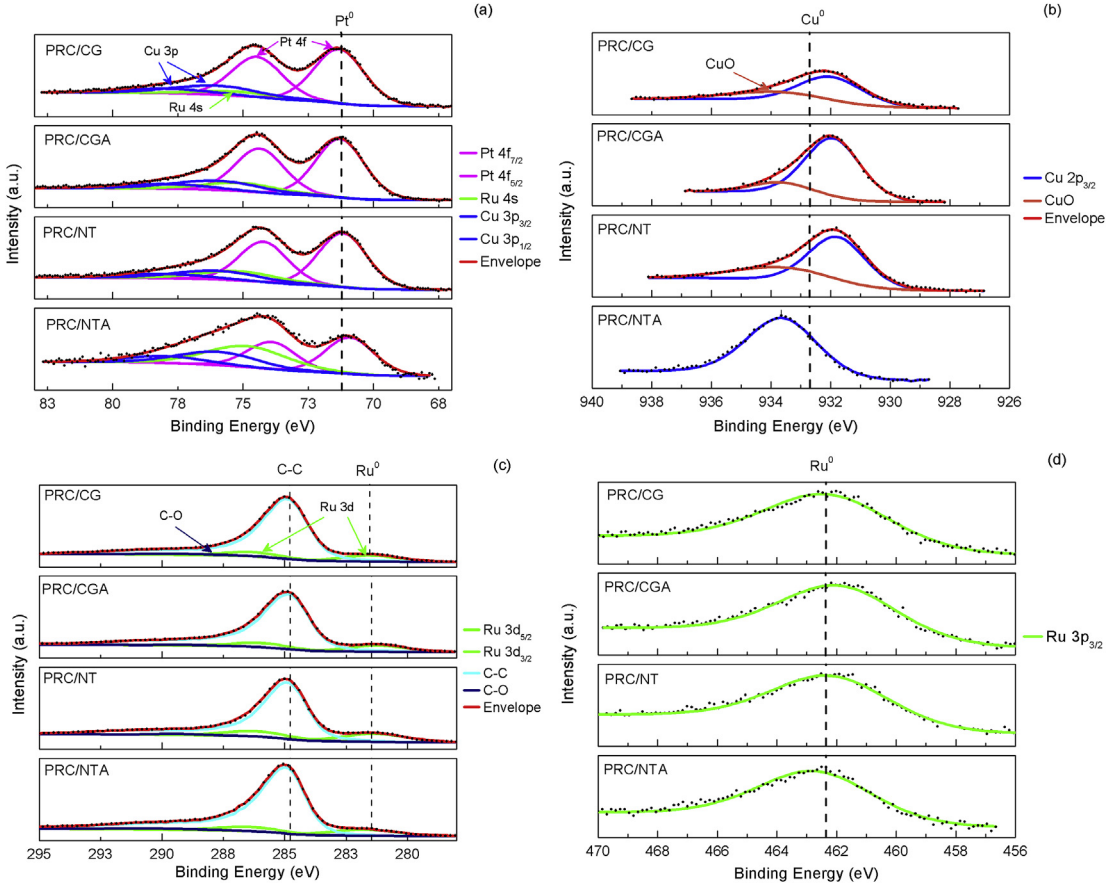

Fig. 4 – XPS profiles of Pt 4f (a), Cu 2p (b), Ru 3d (c) and Ru 3p (d) regions.

energies observed for metallic Cu, indicating an alloy formation with Pt and Ru at the near surface of the nanoparticles. On the other hand, the Cu signal observed for PRC/NTA can be assigned to CuO. Notwithstanding the foregoing, the concentration of CuO in this sample is very small and not detectable by X-ray diffraction. This means that the appearance of cupric oxide on the surface of PRC/NTA catalyst is probably consequence of the sample exposition to atmospheric O_2. The core level spectrum of the Ru 3d region (Fig. 4c) shows a strong overlapped with that corresponding to C 1s. Additionally, the C 1s it is also influenced for the substrate functional groups. Therefore, models peak obtained from pristine substrates were used in order to consider a proper deconvolution of these regions. In this way, the Ru 3d can be deconvoluted into two peaks separated by an energy gap of 5 eV (281.4 and 286.4 eV). On the other hand, the Ru $3p_{3/2}$ region is characterized by a single peak centered at about 462.3 eV (Fig. 4d). This peak can be assigned to the presence of Ru^0 [42,45]. Moreover, a slight band shift of the peak compared to bulk ruthenium can be noted. This result is associated with the electron transfer from Ru to Pt within the solid solution formed at the near surface, since the work function of Pt is larger than that of Ru [46].

Additionally, an enrichment of Pt and Ru at the near-surface of the alloy nanoparticles can be seen from the comparison of EDX and XPS results in Table 3. It is interesting to note that Ru is the major component on the near surface of the nanoparticles, while Pt is the main component of the bulk. This result suggest that during the galvanic displacement reaction the platinum atoms deposited on the surface interdiffuse into the inner of the particle through vacancy defects, while the ruthenium atoms migrate in the opposite direction because of the larger volume fraction and smaller curvature of the outer layers [47]. Another plausible explanation is that the partial dissolution of the surface Cu atoms leaves behind regions of Ru-skeleton structures which are subsequently surrounded by Pt atoms.

Furthermore, CO stripping was used to estimate the electroactive surface area and to obtain information on the surface state of the different catalyst materials. Fig. 5 displays the CO stripping voltammograms recorded at a sweep rate of 10 mV s^{-1} in 0.1 M H_2SO_4 electrolyte. The onset of CO oxidation occurs at 0.18, 0.14, 0.17 and 0.16 V on PRC/CG, PRC/CGA, PRC/NT and PRC/NTA, respectively. The results indicates that the activation treatment of the supports has a small positive impact on the oxidation of carbon monoxide. That is, the electro-oxidation of CO is slightly easier on the oxidized carbon supported nanoparticles than on the pristine carbon supported catalyst. Moreover, two overlapping stripping peaks centered at potentials of about 0.32 and 0.48 V can be observed on all catalysts. Wang and Abruña [48] have indicated that the appearance of multiple peaks during CO oxidation is attributed to different regions (i.e., with different electronic and strain properties) at the catalyst surface, suggesting that the CO_{ad} molecules at defect sites and Pt sites near Ru sites (or in our case Cu-Ru sites) are likely oxidized at low potentials (first peak zone) and these sites can then be covered with OH_{ad} species, which inhibit CO repopulation onto these sites, while the oxidation of CO molecules adsorbed on less active regions (i.e., Pt sites far from Ru/Cu sites or terrace sites) occurs at high potentials (second peak zone). The values of the electroactive surface area per unit mass of catalyst (*ECSA*) are summarized in Table 4. The estimated *ECSA* values were 120 m^2 g^{-1} for PRC/CG, 130.3 m^2 g^{-1} for PRC/CGA, 51.3 m^2 g^{-1} for PRC/NT and 97.2 m^2 g^{-1} for PRC/NTA. The catalyst PRC/CGA presents a minor variation of *ECSA* with respect to PRC/CG (8%), while PRC/NTA exhibits a 53% higher *ECSA* as compared to PRC/NT. The low enhancement in *ECSA* of PRC/CGA can be explained by the combined effect of two phenomena that progress in opposite directions: an increase in nanoparticle size which reduce Pt utilization and an enhancement in the dispersion of the nanoparticles due to the presence of higher amounts of anchoring sites (i.e., oxygen functionalities) for Cu and Ru deposition. On the other hand, the large increase in *ECSA* of PRC/NTA can be attributed to the smaller size and higher dispersion of the supported nanoparticles. Moreover, a significant difference between the shape of the CO stripping curve of NT and those recorded for the other catalysts can be observed. This behavior could be attributed to differences in the surface distribution of the metals at the nanoparticles. The Pt utilization efficiency of all catalysts was also included in Table 4.

Methanol and ethanol electro-oxidation

Fig. 6a and Fig. 6b show the stabilized cyclic voltammetry curves (CV's) recorded for methanol and ethanol electro-oxidation at the different as-prepared electrodes. All curves display a single peak during the positive-going sweep that is characteristic of the electro-oxidation of $MeOH_{ads}$ and $EtOH_{ads}$ molecules on Pt based catalysts. After passing through the maximum, the current density decreases progressively due to platinum oxide formation and then starts to increase again at potentials higher than 0.85 V due to incomplete alcohol oxidation. In the backward scan the corresponding oxidation peak is shifted to a less positive potential (ca. 0.45 V) and the oxidation process proceeds with high reactivation currents. This anodic peak is attributed to the further removal/oxidation of adsorbed by-products and CO, and/or oxidation of alcohol molecules on the freed catalytic sites.

The electrodes present similar onset potentials (E_{onset}) and oxidation peak potentials (E_p) for MOR and EOR. The onset potential for MOR and EOR on PRC/CG and PRC/CGA catalysts occurs at ca. 0.20 V, while the oxidation reactions on PRC/NT and PRC/NTA electrodes take place at about 0.32 V. However, if we look closely at the CV curves in the zone between 0.1 and 0.4 V (inset in Fig. 6a and b), we can noticed that the onset of the reactions for PRC/CGA and PRC/NTA is shifted about 20 mV to a more negative potential with respect to the catalysts prepared with the pristine carbon materials. This result can be explain by the higher amount of oxygen groups on CGA and NTA supports. Besides, the electronic interactions at the metal–support interface decrease the adsorption strength of poisoning species and the oxygen groups facilitate the adsorption of water oxidation intermediates [49,14]. On the other hand, the oxygen moieties also creates lattice strain in the supported nanoparticles. Such lattice compression weakens the bond strength between chemisorbed intermediates and Pt sites [39,50].

Over the entire potential range, the trimetallic alloy particles supported on CG and CGA exhibit about fourfold higher

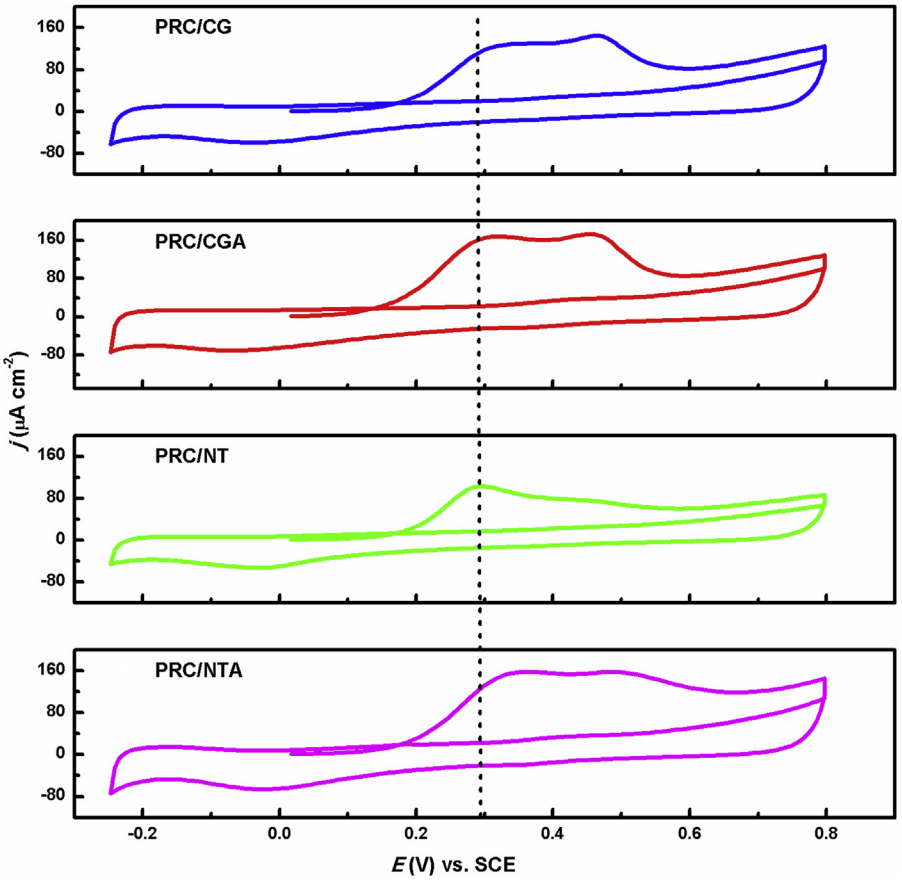

Fig. 5 – Voltammetric curves for adsorbed CO stripping on the as-prepared electrodes in 0.1 M H_2SO_4. $\nu = 10$ mV s^{-1}.

catalytic activities for the electro-oxidation of MeOH and EtOH than those supported on NT and NTA materials. Apart from that, the as-prepared catalysts are more active for the oxidation of ethanol than for the oxidation of methanol. The mass peak current densities for MOR and EOR in the positive going scan were 790 and 1450 A g_{Pt}^{-1} for PRC/CGA, 760 and 1380 A g_{Pt}^{-1} for PRC/CG, 210 and 630 A g_{Pt}^{-1} for PRC/NTA and 170 and 430 A mg_{Pt}^{-1} for PRC/NT. Conversely, the area-normalized peak current densities of PRC/CG and PRC/NT were higher than those of the trimetallic particles supported on the treated carbon materials (Figs. SI1 and SI2). The specific peak current densities for MOR and EOR were 0.33 and 0.57 mA cm^{-2} for PRC/CG, 0.20 and 0.35 mA cm^{-2} for PRC/NT, 0.29 and 0.50 mA cm^{-2} for PRC/CGA and 0.12 and 0.32 mA cm^{-2} for PRC/NTA. Mass activity is related to platinum utilization and to the influence of co-catalysts and the carbonaceous support on the enhancement of the activity, while specific activity is directly related to the number of active sites on the catalyst surface. To explain this contradictory results one must consider that mass activity results from the combination of area activity, platinum utilization and Pt-support interaction as well as co-catalyst effect. Consideration must also be given to the diminution of the electrical conductivity of the supports as a result of the damage (i.e., diminution in the size of the graphitic domains) produced by the oxidative treatment. Taking into account that the electrocatalysts have similar surface composition, it can be thus hypothesized that the mass activity results observed on CV experiments are due to the high Pt utilization efficiency on CGA and NTA and to the enhanced metal-support interaction, which in turn prompts greater

Table 4 – Metal loading and ECSA of the different carbon-supported catalysts.

Sample	[a] Pt loading (μg_{Pt} cm^{-2})	[b] Composition (wt. %)			ECSA (m^2 $g_{catalyst}^{-1}$)	[c] Pt utilization (%)
		Pt	Ru	Cu		
PRC/CG	34.4	50.6	28.5	20.9	120.1	80.0
PRC/CGA	40.7	46.5	24.8	28.7	130.3	99.2
PRC/NT	66.1	61.0	29.2	9.8	51.3	60.0
PRC/NTA	53.8	51.1	29.4	19.5	97.2	92.6

[a] Pt loading from ICP-AES per unit of geometric electrode area.
[b] Metals contents on carbon supports. Data from ICP-AES and EDX analysis.
[c] Pt utilization = (ECSA/CSA) × 100. Chemical surface area (CSA, m^2 g^{-1}) = 6000/(ρ d_p), where ρ is the density of the trimetallic system (g cm^{-3}).

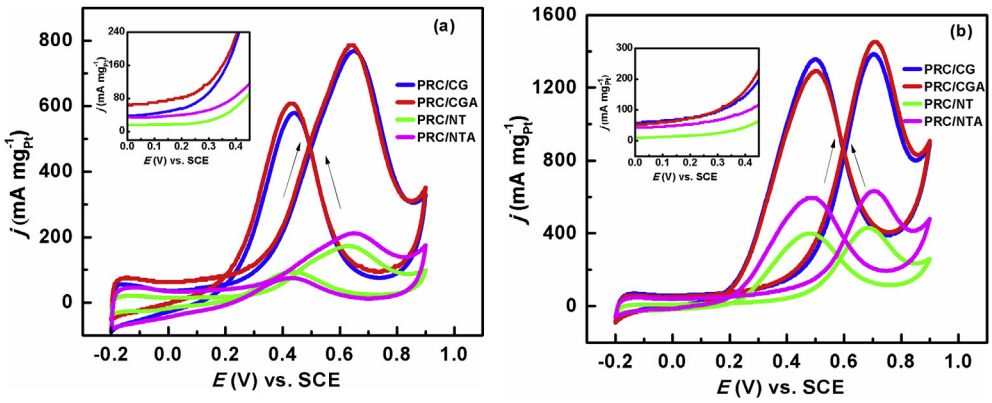

Fig. 6 – Steady cyclic voltammograms for the different electrodes in 1 M CH_3OH/0.5 M H_2SO_4 (a) and 1 M CH_3CH_2OH/0.5 M H_2SO_4 (b). The arrows indicate the scan direction. $\nu = 50$ mV s^{-1}. Current density normalized to the metal loading.

strain and electronic effects in the alloy nanoparticles. In the case of the area-specific activities, it can be said that the inferior performance of PRC/CGA with respect to PRC/CG and of PRC/NTA with respect to PRC/NT electrode may be likely attributed to the reduction of the electrical conductivity of the carbon materials after the oxidative treatment. The enhancement of ECSA after the oxidative treatment of the supports is not enough to compensate the dramatic diminution in the conductivity of the supports. On the other hand, the differences in the mass and area activities between PRC/CG and PRC/NT, and between PRC/CGA and PRC/NTA can be explain by the difference in ECSA and the electrical conductivity of the supports. To sum up, it can be said that the electrocatalytic performance of the trimetallic nanoparticles supported on the as-prepared materials is dependent on the type and amount of surface functionalities, which influence particle size, dispersion and agglomeration extent as well as lattice strain. Moreover, the catalytic activity of the electrodes is strongly influenced by the electrical conductivity of the support. The metal-support interaction, which is different for each support, can also contribute to the observed performance of the as prepared catalysts. The carbon support changes the electronic structure of the trimetallic nanoparticles, thus weakening the binding energy of poisoning intermediates. However, the influence of other important structural characteristics as pore size and pore distribution cannot be entirely ruled out.

To evaluate the catalytic activity under more comparable fuel cell practical conditions, the as-prepared materials were evaluated through potentiostatic tests and compared with the response of a commercial catalyst in the potential region that is relevant to MeOH and EtOH oxidation (Fig. 7 and Fig. SI3). The j vs t curves show that the as-prepared catalysts follow the same trend as that observed in CV experiments. For instance, at 0.4 V PRC/CGA presented the highest mass activity for MeOH and EtOH oxidation in acid medium (201 and 205 A mg_{Pt}^{-1}) followed by PRC/CG (195 and 180 A mg_{Pt}^{-1}), PRC/NTA (26 and 63 A mg_{Pt}^{-1}), and PRC/NT (22 and 54 A mg_{Pt}^{-1}). At the same potential the commercial catalyst developed current densities of 15 and 31 A g_{Pt}^{-1} for MOR and EOR, respectively [23]. Remarkably, the catalytic activity of the trimetallic alloy nanoparticles supported on CGA and CG is about 13 and 7 times higher than that of the commercial system for MOR and EOR, respectively, while in the case of PRC/NTA and PRC/NT the mass current density is increased by 100% with respect to PtRu/C for both MOR and EOR reactions [23].

Furthermore, the poisoning rate (δ) can be calculated from the chronoamperometric measurements by using the following equation [51]:

$$\delta = \frac{100}{I_0}\left(\frac{dI}{dt}\right)_{t>500s} \quad (2)$$

where $(dI/dt)_{t>500}$ is the slope of the linear part of the curve (A s^{-1}) and I_0 is the current determined from the intercept of the regression line with the y-axis (A). The poisoning rates at 0.4 V for MOR and EOR were 0.024 and 0.018% s^{-1} for PRC/CGA, 0.026 and 0.018% s^{-1} for PRC/CG, 0.031 and 0.020% s^{-1} for PRC/NTA and 0.036 and 0.024% s^{-1} for PRC/NT. It is interesting to note that the poisoning rate of the electrodes is influenced by the nature of the carbon support and its degree of interaction with the nanoparticles. On the other hand, the long-term poisoning rates of the home-made electrodes for methanol and ethanol electro-oxidation are between 1.5 and 2 times lower than those of PtRu/C (0.047% s^{-1} for MOR and 0.052% s^{-1} for EOR [23]).

The significant enhancement on the catalytic activity and the improved tolerance to poisoning of the as-synthesized catalysts compared to the commercial electrode can be explained by the larger ECSA of the trimetallic catalysts, the higher Pt utilization efficiency and the modification of the surface electronic structure of Pt due to the shift of Pt d-band position and lattice strain effects, as well as the interaction with carbon support. According to the results, the presence of copper in the trimetallic alloy also plays an important role in the performance of the trimetallic system. On the one hand, the incorporation of Cu atoms causes a reduction of the interatomic Pt-Pt distance and on the other hand modifies the electronic structure of Pt atoms [7], which facilitates the oxidation of adsorbed intermediates.

Finally, the catalytic activity of the most active trimetallic supported electrode was compared with some data available in the literature. The mass activity obtained with PRC/CGA electrode is better than those reported by other authors for MOR and EOR in acid medium. For instance, Wu et al. reported

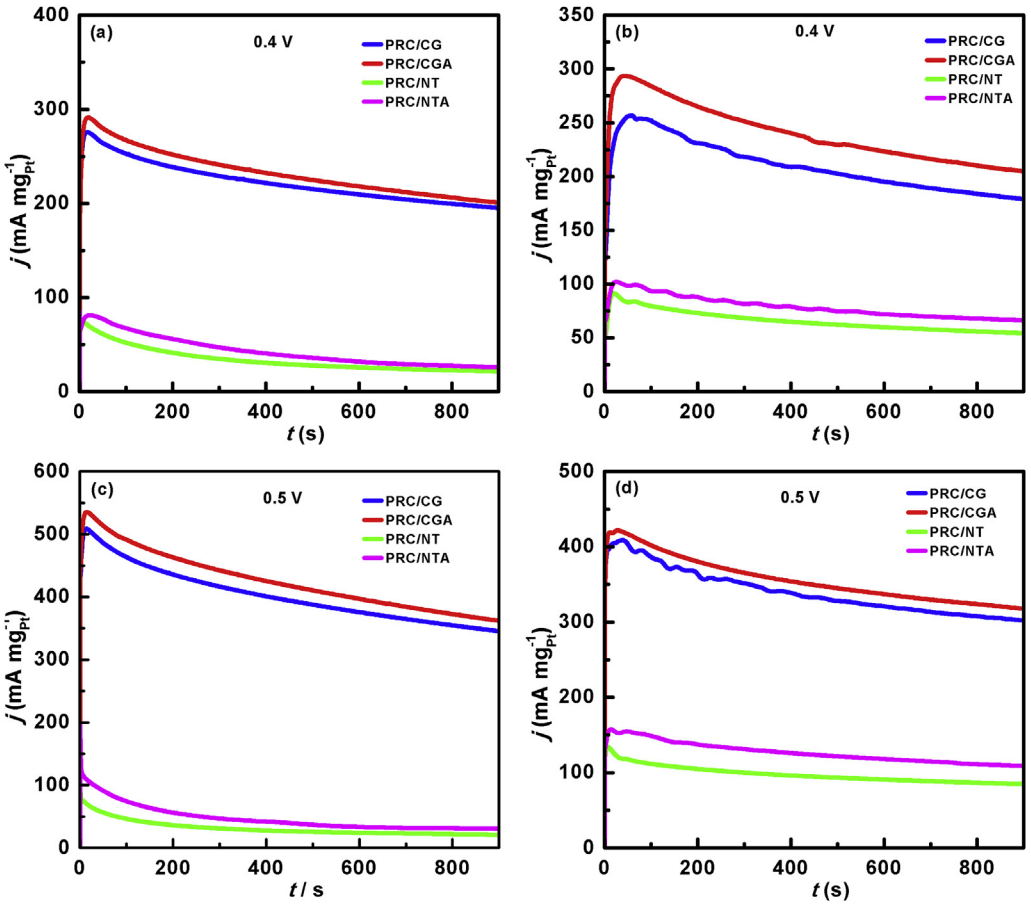

Fig. 7 – Current-time curves at 0.4 and 0.5 V for as-prepared electrodes in 1 M CH_3OH/0.5 M H_2SO_4 (a, c) and 1 M CH_3CH_2OH/0.5 M H_2SO_4 (b, d). Current density normalized to the metal loading.

a catalytic activity of 128 mA mg_{Pt}^{-1} at 0.45 V (vs. SCE) for EOR on a $Pt_{0.5}Sn_{0.5}$/XC-72 electrode (d_p = 2 nm and Pt content = 22 wt %) synthesized using microfluidic reactions in capillary tube reactors [52], while Asgardi et al. reported a current density of 127.8 mA mg_{Pt}^{-1} at 0.31 V (vs. SCE) for EOR on a $Pt_{0.75}Sn_{0.25}$/C electrode (d_p = 4 nm, metal loading = 19 wt % and ECSA = 87.6 $m^2\ g^{-1}$) synthesized via the formic acid method [15]. In another work, Li et al. reported that a Pt catalyst (d_p = 5 nm, ECSA = 26 $m^2\ g^{-1}$ and Pt loading = 25 wt %) supported on a VulcanXC72R-copper phosphide (1:1) composite showed a catalytic activity of about 106 and 75 mA mg_{Pt}^{-1} at 0.6 V (vs. SCE) for MOR and OER, respectively [53]. Recently, Poochai et al. stated a catalytic activity of 54 mA mg_{Pt}^{-1} at 0.46 V (vs. SCE) for MOR on a Cu@PtRu core-shell catalyst (d_p = 9.6 nm and ECSA = 31.3 $m^2\ g_{Pt}^{-1}$) supported over a carbon paper [54]. Cao et al. [11] studied the electro-oxidation of methanol in acid medium onto hierarchical branched Pt–Cu nanoparticles (d_p = 30 nm and ECSA = 51.6 $m^2\ g^{-1}$). The authors obtained a catalytic activity of 97.6 mA mg_{Pt}^{-1} at 0.57 V (vs. SCE). In general terms, one could say that the as-prepared trimetallic PtRuCu catalysts can be considered as a promising anodic material for direct alcohols fuel cells. Further investigations in our research group are ongoing to evaluate the role of the textural and structural properties of ordered mesoporous carbons and biocarbons on the electrocatalytic properties of nanostructured particles with low Pt content towards ethanol oxidation.

Conclusions

The present study was designed to determine the influence of the nature and surface state of the carbon support on the electrocatalytic activity of trimetallic alloy nanoparticles synthesized by a two-step route for methanol and ethanol oxidation in acid medium. PtRuCu particles between 3 and 4 nm in size were deposited over pretreated or pristine carbon black and multiwalled carbon nanotubes materials. The different physicochemical and electrochemical analysis indicated that the metals are forming PtRuCu solid solution alloy nanoparticles. XRD and TEM results pointed out that the nature and state of the support have an important influence in lattice strain, size and distribution of the trimetallic nanoparticles. Besides, XPS results indicated that a strong electronic interaction exists between the surface and the carbon support. Cyclic voltammetry and chronoamperometry were employed to evaluate the catalytic performance of the supported trimetallic alloy nanoparticles for MOR and EOR. The results indicated that the activated carbon black supported trimetallic PtRuCu catalyst exhibits the best performance for

methanol and ethanol oxidation in terms of onset potential, poisoning rate and mass activity. Furthermore, the pristine and treated carbon black supported PtRuCu catalysts exhibited about fourfold higher catalytic activities for MOR and EOR than those of pristine and treated MWCNTs supported PtRuCu catalysts. These results can be explained in part by the metal-support interaction and Pt utilization efficiency. The different electrical conductivity of the supports can also contributes to explain this behavior.

On the other hand, the activity of the trimetallic alloy nanoparticles supported on activated carbon black is 13 and 7 times higher than that of a commercial PtRu/C catalyst for MOR and EOR at 0.4 V, respectively. Furthermore, the poisoning rates for both alcohols was about 1.5 times lower than that of the commercial material. Based on these results, the activated carbon black supported trimetallic PtRuCu electrode seems to be a promising anodic material for direct alcohols fuel cells.

Acknowledgements

This work was supported by ANPCYT grants PICT2013 N°2370 and PICT2014 N° 3393 and Universidad Nacional del Sur grant PGI 24/M142. V.C. thanks CONICET for a doctoral fellowship.

Appendix A. Supplementary data

Supplementary data related to this article can be found at http://dx.doi.org/10.1016/j.ijhydene.2017.08.079.

REFERENCES

[1] Corti HR, Gonzalez ER, editors. Direct alcohol fuel cells: materials, performance, durability and applications. Dordrecht, The Netherlands: Springer; 2014.
[2] Rodríguez LA, Toro ME, Vazquez F, Correa-Daneri ML, Gouiric SC, Vallejo MD. Bioethanol production from grape and sugar beet pomaces by solid-state fermentation. Int J Hydrogen Energy 2010;35:5914–7.
[3] Petrou EC, Pappis CP. Bioethanol production from cotton stalks or corn Stover? A comparative study of their sustainability performance. ACS Sustain Chem Eng 2014;2:2036–41.
[4] Solomon B, Luzadis VA, editors. Renewable energy from forest resources in the United States. New York, USA: Routledge; 2009.
[5] Kakaç S, Pramuanjaroenkij A, Vasiliev L, editors. Mini-micro fuel cells: fundamentals and applications. Dordrecht, The Netherlands: Springer; 2008.
[6] Brouzgou A, Podias A, Tsiakaras P. PEMFCs and AEMFCs directly fed with ethanol: a current status comparative review. J Appl Electrochem 2013;43:119–36.
[7] Strasser P, Koh S, Anniyev T, Greeley J, More K, Yu C, et al. Lattice-strain control of the activity in dealloyed core–shell fuel cell catalysts. Nat Chem 2010;2:454–60.
[8] Stamenkovic VR, Mun BS, Mayrhofer KJJ, Ross PN, Markovic NM. Effect of surface composition on electronic structure, stability, and electrocatalytic properties of Pt transition metal alloys: Pt-skin versus Pt-skeleton surfaces. J Am Chem Soc 2006;128:8813–9.
[9] Xie J, Zhang Q, Gu L, Xu S, Wang P, Liu J, et al. Ruthenium–platinum core–shell nanocatalysts with substantially enhanced activity and durability towards methanol oxidation. Nano Energy 2016;21:247–57.
[10] Huang M, Wu C, Guan L. Chemical corrosion of PtRuCu6/C for highly efficient methanol oxidation. J Power Sources 2016;306:489–94.
[11] Cao Y, Yang Y, Shan Y, Huang Z. One-pot and facile fabrication of hierarchical branched Pt–Cu nanoparticles as excellent electrocatalysts for direct methanol fuel cells. ACS Appl Mater Interfaces 2016;8:5998–8:59. Lee Y-W, Lee J-Y, Kwak D-H, Hwang E-T, Sohn JI, Park K-W. Pd@Pt core–shell nanostructures for improved electrocatalytic activity in methanol oxidation reaction. Appl Catal B 2015;179:178–84.
[12] Cheng Y, Shen PK, Jiang SP. Enhanced activity and stability of core-shell structured $PtRuNi_x$ electrocatalysts for direct methanol fuel cells. Int J Hydrogen Energy 2016;41:1935–43.
[13] Ma J, Habrioux A, Gago AS, Alonso-Vante N. Towards understanding the essential role played by the platinum-support interaction on electrocatalytic activity. ECS Trans 2013;45:25–33.
[14] Sieben JM, Duarte MME, Mayer CE. Electro-oxidation of methanol on Pt-Ru nanostructured catalysts electrodeposited onto electroactivated carbon fiber materials. ChemCatChem 2010;2:182–9.
[15] Asgardi J, Calderón JC, Alcaide F, Querejeta A, Calvillo L, Lázaro MJ, et al. Carbon monoxide and ethanol oxidation on PtSn supported catalysts: effect of the nature of the carbon support and Pt:Sn composition. Appl Catal B 2015;168-169:33–41.
[16] Zhang L-M, Sui X-L, Zhao L, Zhang J-J, Gu D-M, Wang Z-B. Nitrogen-doped carbon nanotubes for high-performance platinum-based catalysts in methanol oxidation reaction. Carbon 2016;108:561–7.
[17] Alegre C, Sebastián D, Gálvez ME, Moliner R, Lázaro MJ. Sulfurized carbon xerogels as Pt support with enhanced activity for fuel cell applications. Appl Catal B 2016;192:260–7.
[18] Viva FA, Bruno MM, Jobbágy M, Corti HR. Electrochemical characterization of PtRu nanoparticles supported on mesoporous carbon for methanol electrooxidation. J Phys Chem C 2012;116:4097–104.
[19] Sieben JM, Comignani V, Alvarez AE, Duarte MME. Synthesis and characterization of Cu core Pt-Ru shell nanoparticles for the electro-oxidation of alcohols. Int J Hydrogen Energy 2014;39:8667–74.
[20] Nieva Lobos ML, Sieben JM, Comignani V, Duarte M, Volpe MA, Moyano EL. Biochar from pyrolysis of cellulose: an alternative catalyst support for the electro-oxidation of methanol. Int J Hydrogen Energy 2016;41:10695–706.
[21] Marinho B, Ghislandi M, Tkalya E, Koning CE, de With G. Electrical conductivity of compacts of graphene, multi-wall carbon nanotubes, carbon black, and graphite powder. Powder Technol 2012;221:351–8.
[22] Celzard A, Marêché JF, Payot F, Furdin G. Electrical conductivity of carbonaceous powders. Carbon 2002;40:2801–15.
[23] Sieben JM, Alvarez AE, Comignani V, Duarte MME. Methanol and ethanol oxidation on carbon supported nanostructured Cu core Pt-Pd shell electrocatalysts synthesized via redox displacement. Int J Hydrogen Energy 2014;39:11547–56.
[24] Comignani V, Sieben JM, Brigante ME, Duarte MME. Carbon supported Pt-NiO nanoparticles for ethanol electro-oxidation in acid media. J Power Sources 2015;278:119–27.
[25] Soboleva T, Zhao X, Malek K, Xie Z, Navessin T, Holdcroft S. On the micro-, meso-, and macroporous structures of

polymer electrolyte membrane fuel cell catalyst layers. ACS Appl Mater Interfaces 2010;2:375–84.
[26] Li F, Wang Y, Wang D, Wei F. Characterization of single-wall carbon nanotubes by N_2 adsorption. Carbon 2004;42:2375–83.
[27] Senthil Kumar SM, Soler Herrero J, Irusta S, Scott K. The effect of pretreatment of Vulcan XC-72R carbon on morphology and electrochemical oxygen reduction kinetics of supported Pd nano-particle in acidic electrolyte. J Electroanal Chem 2010;647:211–21.
[28] Raymundo-Piñero E, Azaïs P, Cacciaguerra T, Cazorla-Amorós D, Linares-Solano A, Béguin F. KOH and NaOH activation mechanisms of multiwalled carbon nanotubes with different structural organization. Carbon 2005;43:786–95.
[29] Aksoylu AE, Freitas MMA, Figueiredo JL. Bimetallic Pt–Sn catalysts supported on activated carbon I. The effects of support modification and impregnation strategy. Appl Catal A 2000;192:29–42.
[30] Boyano A, Herrera C, Larrubia MA, Alemany LJ, Moliner R, Lázaro MJ. Vanadium loaded carbon-based monoliths for the on-board no reduction: influence of temperature and period of the oxidation treatment. Chem Eng J 2010;160:623–33.
[31] Chingombe P, Saha B, Wakeman RJ. Surface modification and characterisation of a coal-based activated carbon. Carbon 2005;43:3132–43.
[32] Lennon D, Lundie DT, Jackson SD, Kelly GJ, Parker SF. Characterization of activated carbon using x-ray photoelectron spectroscopy and inelastic neutron scattering spectroscopy. Langmuir 2002;18:4667–73.
[33] Kundu S, Wang Y, Xia W, Muhler M. Thermal stability and reducibility of oxygen-containing functional groups on multiwalled carbon nanotube surfaces: a quantitative high-resolution XPS and tpd/tpr study. J Phys Chem C 2008;112:16869–78.
[34] Gallagher KG, Yushin G, Fuller TF. The role of nanostructure in the electrochemical oxidation of model-carbon materials in acidic environments. J Electrochem Soc 2010;157:B820–30.
[35] Cochell T, Manthiram A. Pt@PdxCuy/C Core-Shell electrocatalysts for oxygen reduction reaction in fuel cells. Langmuir 2012;28:1579–87.
[36] Xing Y, Cai Y, Vukmirovic MB, Zhou W-P, Karan H, Wang JX, et al. Enhancing oxygen reduction reaction activity via Pd-Au alloy sublayer mediation of Pt monolayer electrocatalysts. J Phys Chem Lett 2010;1:3238–42.
[37] Montes de Oca MG, Kumarakuru H, Cherns D, Fermín DJ. Hydrogen adsorption at strained Pd nanoshells. J Phys Chem C 2011;115:10489–96.
[38] Daio T, Staykov A, Guo L, Liu J, Tanaka M, Lyth SM, et al. Lattice strain mapping of platinum nanoparticles on carbon and SnO_2 supports. Sci Rep 2015;5:13126.
[39] Chastain J, editor. Handbook of x-ray photoelectron spectroscopy. USA: Perking-Elmer Corporation; 1992.
[40] Selvarani G, Maheswari S, Sridhar P, Pitchumani S, Shukla AK. Carbon-supported Pt–TiO2 as a methanol-tolerant oxygen-reduction catalyst for DMFCs. J Electrochem Soc 2009;156:B1354–60.
[41] Wang H, Wang R, Li H, Wang Q, Kang J, Lei Z. Facile synthesis of carbon-supported pseudo-core@shell PdCu@Pt nanoparticles for direct methanol fuel cells. Int J Hydrogen Energy 2011;36:839–48.
[42] Bock C, Paquet C, Couillard M, Botton GA, MacDougall BR. Size-selected synthesis of PtRu nano-catalysts: reaction and size control mechanism. J Am Chem Soc 2004;126:8028–37.
[43] Sarkar A, Manthiram A. Synthesis of Pt@Cu core-shell nanoparticles by galvanic displacement of Cu by Pt4+ ions and their application as electrocatalysts for oxygen reduction reaction in fuel cells. J Phys Chem C 2010;114:4725–32.
[44] Zhou J, Zhou X, Sun X, Li R, Murphy M, Ding Z, et al. Interaction between Pt nanoparticles and carbon nanotubes – an Xray absorption near edge structures (XANES) study. Chem Phys Lett 2007;437:229–32.
[45] Guo JW, Zhao TS, Prabhuram J, Chen R, Wong CW. Preparation and characterization of a PtRu/C nanocatalyst for direct methanol fuel cells. Electrochim Acta 2005;51:754–76.
[46] Watanabe M, Uchida H. Electrocatalysis at platinum and bimetallic alloys. In: Koper MTM, editor. Fuel cell catalysis: a surface science approach. New Yersey: John Wiley & Sons; 2009. p. 317–41.
[47] Shibata T, Bunker BA, Zhang Z, Meisel D, Vardeman CF, Gezelter JD. Size-dependent spontaneous alloying of Au-Ag nanoparticles. J Am Chem Soc 2002;124:11989–96.
[48] Wang H, Abruña HD. Origin of multiple peaks in the potentiodynamic oxidation of CO adlayers on Pt and Ru-Modified Pt electrodes. J Phys Chem Lett 2015;6:1899–906.
[49] Lu X, Yim W-L, Suryanto BHR, Zhao C. Electrocatalytic oxygen evolution at surface-oxidized multiwall carbon nanotubes. J Am Chem Soc 2015;137:2901–7.
[50] Celorrio V, Montes de Oca MG, Plana D, Moliner R, Lazaro MJ, Fermín DJ. Effect of carbon supports on electrocatalytic reactivity of Au–Pd Core–Shell nanoparticles. J Phys Chem C 2012;116:6275–82.
[51] Jiang J, Kucernak A. Electrooxidation of small organic molecules on mesoporous precious metal catalysts II: CO and methanol on platinum/ruthenium alloy. J Electroanal Chem 2003;543:187–99.
[52] Wu F, Zhang D, Peng M, Yu Z, Wang X, Guo G, et al. Microfluidic synthesis enables dense and uniform loading of surfactant-free PtSn nanocrystals on carbon supports for enhanced ethanol oxidation. Angew Chem Int Ed 2016;55:4952–6.
[53] Li R, Ma Z, Zhang F, Meng H, Wang M, Bao X-Q, et al. Facile Cu_3P-C hybrid supported strategy to improve Pt nanoparticle electrocatalytic performance toward methanol, ethanol, glycol and formic acid electro-oxidation. Electrochim Acta 2016;220:193–204.
[54] Poochai C, Veerasai W, Somsook E, Dangtip S. Dealloyed ternary Cu@Pt-Ru core-shell electrocatalysts supported on carbon paper for methanol electrooxidation catalytic activity. Electrochim Acta 2016;222:1243–56.